

Article

Energy Saving Evaluation of the Ventilated BIPV Walls

Chi-Ming Lai ^{1,2,*} and Yi-Pin Lin ³

¹ Research Center for Energy Technology and Strategy, National Cheng Kung University, Taiwan/1, University Road, Tainan City 701, Taiwan

² Department of Civil Engineering, National Cheng Kung University, Taiwan/1, University Road, Tainan City 701, Taiwan

³ Department of Interior Design, Tung Fang Design University, Taiwan/110, Dong fang Road, Hunei District, Kaohsiung City 82941, Taiwan; E-Mail: purple5028@gmail.com

* Author to whom correspondence should be addressed; E-Mail: cmlai@mail.ncku.edu.tw; Tel.: +886-6-2757575 (ext. 63136); Fax: +886-6-2090569.

Received: 17 January 2011; in revised form: 30 May 2011 / Accepted: 10 June 2011 /

Published: 14 June 2011

Abstract: This study integrates photovoltaic (PV) system, building structure, and heat flow mechanism to propose the notion of ventilated Building-Integrated Photovoltaic (BIPV) walls. The energy-saving potential of the ventilated BIPV walls was investigated via engineering considerations and computational fluid dynamics (CFD) simulations. The results show that the heat removal rate and indoor heat gain of the proposed ventilated BIPV walls were dominantly affected by outdoor wind velocity and airflow channel width. Correlations for predicting the heat removal rate and indoor heat gain, the reduction ratio of the indoor heat gain, CO₂ reduction, and induced indoor air exchange are introduced.

Keywords: energy; BIPV; building; CFD

1. Introduction

Building-Integrated Photovoltaics (BIPV) refers to an architectural design approach that combines photovoltaic (PV) panels with the building construction system. This combination allows BIPV to not only feature a power generation function but also to become part of the building façade. However, solar irradiation, received by PV cells, would be transformed into heat and cause an increase of the PV

cell temperature, which is associated with the generation efficiency. Dubey and Tiwari showed that the increase in cell temperature decreases the cell efficiency and at the end of the day it will again increase due to the decrease in cell temperature [1]. Therefore, whenever possible, it is necessary to fully enhance a PV's heat dissipation. Because an irradiated PV panel is a heat source in the BIPV construction, a double-skin design concept can possibly be used to design the BIPV structure as a ventilated BIPV.

The ventilated BIPV design strategy can be achieved through a double-skin design, known as an effective way to reduce a building's solar heat gain [2,3]. A double-skin structure enables the mezzanine to form an air layer. In the summer months, an air layer with open ends can reduce the heat entering into the room. After radiation heat has reached the double-skin, it will heat the trapped air to generate a natural convection flow. This type of airflow can remove part of the indoor heat energy and reduce the indoor heat gain, thereby reducing HVAC cooling load. Ventilated BIPV can also induce indoor ventilation. The environmental control effect of a double-skin design includes:

(1) To become a static air insulation

In cold regions, multi windows and multi exterior wall structures can be seen, which take advantage of the fact that the air layer in a double-skin construction can be used to withstand the chilly winter.

(2) To take advantage of outdoor wind force to initiate the indoor ventilation mechanism through the double-skin channel.

(3) Solar Chimney

Buoyancy effect, caused by the solar heat-gain, becomes the driving force to induce the air flow in the double-skin channel, so as to achieve the effect of ventilation and heat transfer. The location and function can:

(i) continue the structure of a conventional chimney [4]

(ii) be combined with exterior walls

Setting a translucent panel at the outermost part of the building structure allows the solar radiation to penetrate, and then there will be an air channel between the exterior wall and the newly-set translucent panel. The sunshine can directly irradiate on the exterior wall, which makes the air around the exterior wall create a thermal buoyancy flow [5].

(iii) combined with a pitched roof

Khedari *et al.* [6] established a solar chimney mixed with pitch roof (Roof Solar Collector, RSC) and three solar chimneys mixed with external walls, including Trombe Wall (TW), Modified Trombe (MTW) and Metallic Solar Wall (MSW), to investigate the energy-saving efficiency with an individual 6–9 m² testing area. Chen *et al.* [7] used model experiments to explore the airflow phenomena within the solar chimney of a pitched roof through a smoke tracing method. Del Coz Diaz *et al.* [8] studied the performance of a ventilated self-weighted wood panel used on ventilated roofs, carrying out a convective heat transfer analysis of the panel by the finite volume method (FVM). Design verification and advantage of the FVM over the finite element method were explored.

(iv) use independent structures

Aboulnaga [9] made an independent solar chimney which is very similar to the former pitched roof structure. The slope of this kind of solar chimney should be between 25 and 30 degrees.

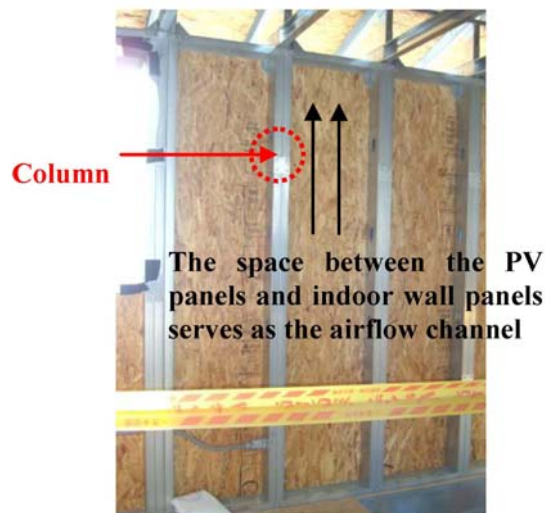
The design logic of a ventilated BIPV in hot and humid area includes: (1) considering a possible PV panel structure to function as the building skin, (2) blending the PV panels into the building construction system to achieve BIPV, (3) allowing the BIPV structure to have the capability of self-environmental control to reduce the impact caused by increased temperatures and (4) using the environmental control design approach to enable BIPV to induce indoor ventilation and reduce the cooling load. There is still limited existing literature on ventilated BIPV effectiveness on solar heat removal, and a lack of similar ventilated BIPV structures. This study aims to understand the thermal effect on the innovative BIPV module and to explore the use of thermal management to decrease the thermal impact. An innovative ventilated BIPV wall design is proposed and evaluated via engineering considerations and computational fluid dynamics (CFD) simulations.

2. Research Methods

2.1. Design Development

Before establishing the physical model, we must first explore a practical method for replacing a standard existing exterior wall with ventilated BIPV construction. In Taiwan, residential buildings are often composed of reinforced concrete or light steel. A conventional exterior wall structure for a light steel house is shown in Figure 1. In such constructions, C-shaped or square steel studs are erected to be the main support where outdoor and indoor wall panels are attached.

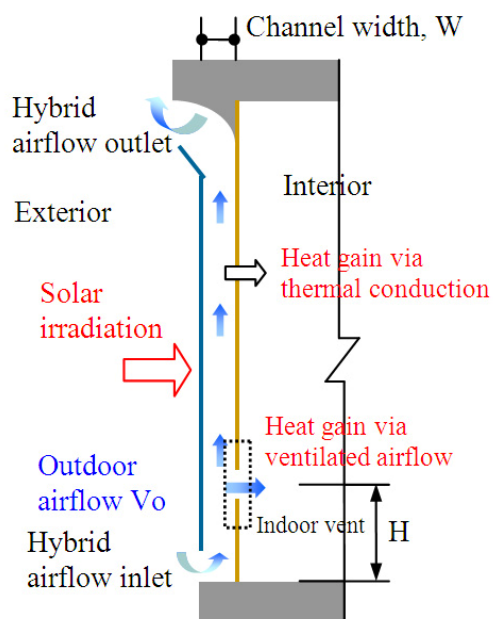
Figure 1. The exterior wall structure of a light steel house.



As shown in Figure 2, this study suggests the replacement of the exterior wall panels with PV panels, leaving the space between the exterior and interior walls as an airflow channel to provide natural ventilation and heat dissipation for the ventilated BIPV wall. The channel space, which has the same dimensions as the column width, can also be used for installation of PV cables. Each row of PV

panels (*i.e.*, every external wall unit divided by two columns) has an air inlet at its base. The outdoor airflow enters through the inlet into the mezzanine channel, which is formed by the PV panels and indoor decorative boards. After flowing through the entire row of PV panels, the airflow in the channel is discharged from the outlet located on top of the PV panels. A detailed design of the outlet vent has been simulated using CFD technology to ensure that the outdoor airflow will not flow in through the top air vent and reduce the strength of the buoyancy.

Figure 2. The ventilated BIPV wall proposed in this study.



2.2. Physical Model

The investigated model space has the dimensions 6.1 m (L) \times 3.2 m (W) \times 2.85 m (H) and the exterior wall of the house is designed as the ventilated BIPV wall, shown in Figure 3. The main parameters for the model space used for the study are detailed in Table 1 and illustrated in Figure 3.

Figure 3. Schematic diagram of the proposed ventilated BIPV and investigated space.

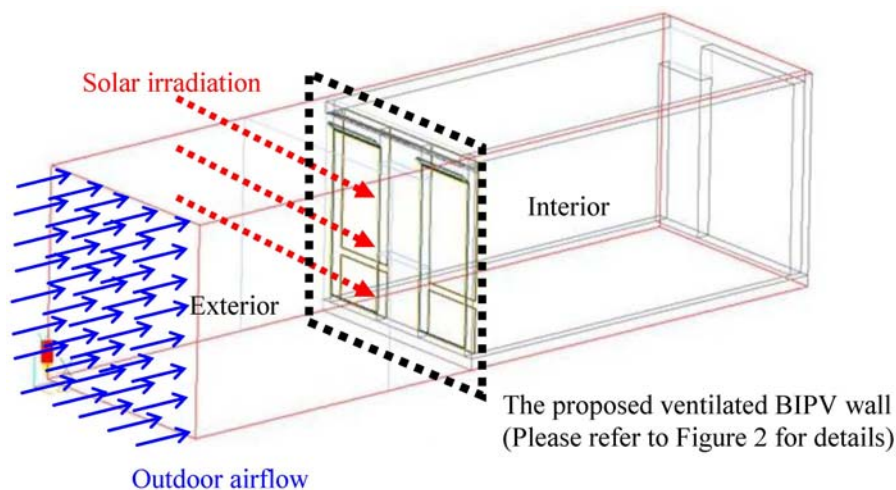


Table 1. Main parameters for the CFD simulations.

	Item	Settings
1. Outdoor environment	(Typical weather conditions in Taiwan)	Fix the outdoor air temperature at 29 °C Fix the solar irradiation at 600 W/m ² Change the air velocity V_o (0.5, 1.0, 2.0 m/s)
2. Exterior wall	Original exterior wall location	Replace the original exterior wall with the proposed ventilated BIPV wall
	BIPV airflow channel width	Change the airflow channel width W (5, 10, 15, 20 cm) (Change under the premise of meeting the actual exterior wall structure of the building)
	Indoor vent	Fix the opening area Change the opening height H (15, 30, 45, 60, 75, 90 cm) (Under the premise of meeting the actual interior design)
	Thermal properties	PV panel: $k = 60$ W/mK; $\rho = 7854$ kg/m ³ ; $C_p = 434$ J/kg K indoor wall panel (wood): $k = 0.16$ W/mK; $\rho = 720$ kg/m ³ ; $C_p = 1255$ J/kg K
3. Indoor space	Indoor furniture	No furnishings
	Indoor heat source	No indoor heat source
4. Indoor partition wall		Close the door (ignore cracks in interior door) Adiabatic wall

2.3. Numerical Method

Numerical simulations of the physical problem under consideration were performed using a finite volume method to solve the governing equations and boundary conditions mentioned above. A CFD code, PHOENICS, was used to simulate the airflow and temperature distributions. The governing equations solved by PHOENICS include the three-dimensional time-dependent incompressible Navier-Stokes equation, the time-dependent convection diffusion equation and k - ϵ turbulence equations. These formulated equations can be found in the PHOENICS user's manual [10] and in any CFD textbook. For the k - ϵ turbulence equation, the empirical turbulence coefficients were assigned as $\sigma_k = 1.0$, $\sigma_\epsilon = 1.22$, $\sigma_{\epsilon 1} = 1.44$, $\sigma_{\epsilon 2} = 1.92$, and $C_\mu = 0.09$. These values were widely accepted in the CFD k - ϵ model. To bridge the steep dependent variable gradients close to the solid surface, the general wall function was employed. The iterative calculation was continued until a prescribed relative convergence of 10^{-3} was satisfied for all the field variables of this problem. The numerical simulation accuracy depends on the resolution of the computational mesh, and a finer grid leads to more accurate solutions. In this study, a grid system with approximately $52 \times 162 \times 120$ cells was used for the numerical simulation. Increasing the number of cells will provide information that is more accurate. However, increasing the number of cells will also increase the computation resources required.

2.4. Evaluation Indicators

2.4.1. Heat Removal Rate

When sunlight radiates onto the ventilated BIPV wall, thermal energy will be absorbed, causing the temperature of the PV panels to rise and the air in the airflow channel to be heated. These reactions will generate buoyancy to push up the channel air and remove part of the heat via a natural convection

mechanism. The other part of the heat energy will be transmitted into the indoor space by means of thermal conduction through the interior wall panels of the BIPV structure. Furthermore, the outdoor air can also flow into the airflow channel of the ventilated BIPV wall through the inlet below the BIPV structure to generate forced convection and remove the heat gain on the PV panels. A mixed convection mechanism is generated within the airflow channel. By measuring the temperature and airflow rate, the amount of the heat transfer rate \dot{Q}_{ch} (W) that has been carried away by convective airflow in the channel can be calculated as shown in Equation (1).

$$\dot{Q}_{ch} = \dot{m}C_p(T_{m,o} - T_{m,i}) \quad (1)$$

where \dot{m} is the mass flow rate (kg/s) of the channel airflow, $\dot{m} = \rho V_{m,o} A_c$, ρ is the air density (kg/m³), $V_{m,o}$ is the average velocity (m/s) at the outlet of channel airflow, A_c is the cross-sectional area of the channel (m²), C_p is the air specific heat (J/kg °C), $T_{m,o}$ is the average air temperature at the outlet, and $T_{m,i}$ is the average air temperature (°C) at the inlet.

2.4.2. Energy-Saving

Solar radiation penetrates a building's opening directly to heat the indoor air or indoor facilities. It is also able to heat the outdoor air or exterior walls to transmit thermal energy through the building skin. Indoor heat gain is a result of these two phenomena. The indoor heat gain \dot{Q}_{in} induced by the ventilated BIPV wall can be calculated from Equation (2) as:

$$\dot{Q}_{in} = \dot{Q}_{cond} + \dot{Q}_{vent} \quad (2)$$

where \dot{Q}_{cond} is the rate of conductive heat transfer (W) transmitted through the interior wall panels of the ventilated BIPV to the indoor air, and \dot{Q}_{vent} is the heat gain (W) that flowed in through the indoor vent:

$$\dot{Q}_{cond} = \frac{k}{d}(T_L - T_R)As \quad (3)$$

where k is the thermal conductivity (W/m °C) of the interior wall panels of the ventilated BIPV, d is the thickness of the interior wall panel, T_L and T_R are the wall surface temperature (°C) of the interior wall panels, and As is the area of the interior wall panel (m²):

$$\dot{Q}_{vent} = \dot{m}_v C_p (T_v - T_r) \quad (4)$$

where \dot{m}_v is the air mass flow rate (kg/s) that flowed through the indoor vent, T_v is the average air temperature (°C) at the indoor vent, and T_r is the initial temperature (°C) of the indoor air.

To investigate the indoor heat gain difference between the ventilated BIPV wall and the conventional exterior wall, the heat transfer rate \dot{Q}_w of the RC exterior wall structure or the exterior steel wall was calculated using Equation (5):

$$\dot{Q}_w = U(T_i - T_o)A_w \quad (5)$$

where U is the overall heat transfer coefficients (W/m² °C) of the exterior walls of RC buildings or light steel houses, T_i and T_o are the surface temperatures (°C) on both sides of the RC or steel wall

surface, and A_w is the total surface area (m^2) of the exterior wall. The reduction ratio of the indoor heat gain (η) was estimated using Equation (6). Thermal properties of each individual layer of the exterior walls for calculating the U values were listed Figure 4:

$$\eta = \frac{\dot{Q}_{in} - \dot{Q}_w}{\dot{Q}_w} \quad (6)$$

Figure 4. Thermal properties of each individual layer of the exterior walls.

	Tile	Mortar	RC	Mortar
Thickness(mm)	10	15	120	10
Density (kg/m^3)	2400	2000	2200	2000
Specific heat ($kJ/kg K$)	0.84	0.8	0.88	0.8
Thermal conductivity ($W/m K$)	1.3	1.5	1.4	1.5

(a) Exterior wall of RC buildings

	Al panel	Rock wool	Air	Sodium Calcium plate
Thickness (mm)	6	20	20	25
Density (kg/m^3)	2700	1200	1.6	900
Specific heat ($kJ/kg K$)	0.9	0.84	0.84	0.63
Thermal conductivity ($W/m K$)	210	0.051	0.11	0.15

(b) Exterior wall of light steel houses

2.4.3. CO₂ Reduction

Based on the electricity emission factor of 0.623 kg CO₂^e/kW-h provided by the Bureau of Energy, Ministry of Economic Affairs in Taiwan, the CO₂ reduction effect of the developed ventilated BIPV can be calculated.

3. Results and Discussion

3.1. Heat Removal Rate and Indoor Heat Gain of the Ventilating BIPV Wall

The CFD simulations were conducted under the conditions of three outdoor wind velocities, four airflow channel widths and six indoor vent heights, as listed in Table 1. Airflow simulations of different airflow channel widths ($V_o = 0.5$ m/s and $H = 45$ cm) are shown in Figures 5. The results showed that when the outdoor airflow entered the inlet of the ventilated BIPV wall, part of the airflow would enter indoor through the indoor vent, and part of it would flow upward and out through the top outlet which would also be entrained by the outdoor airflow around the outlet. When the flow channel was widened, besides an upward airflow with a hydraulic jump around the channel lower part, part of the channel airflow would enter the indoor vent in an upward slanting manner, enhancing the indoor vent flow.

Figure 6 illustrated CFD simulations of temperature distributions (cases with $H = 45$ cm). It was obvious that the thermal boundary layer thickness was controlled to a certain extent, with exception of the area near the outlet. The thickness was able to be controlled even for cases with strong buoyancy. The thermal boundary layer development prevented the solar heat flow from entering indoors through the designed BIPV wall. When the outdoor air velocity increased, the forced convection in the channel also increased, and the thermal boundary layer thickness decreased. Due to space limitation of the article, the introduction on other CFD simulation results is omitted.

Figure 5. CFD simulations of flow patterns (cases with $V_o = 0.5$ m/s and $H = 45$ cm).

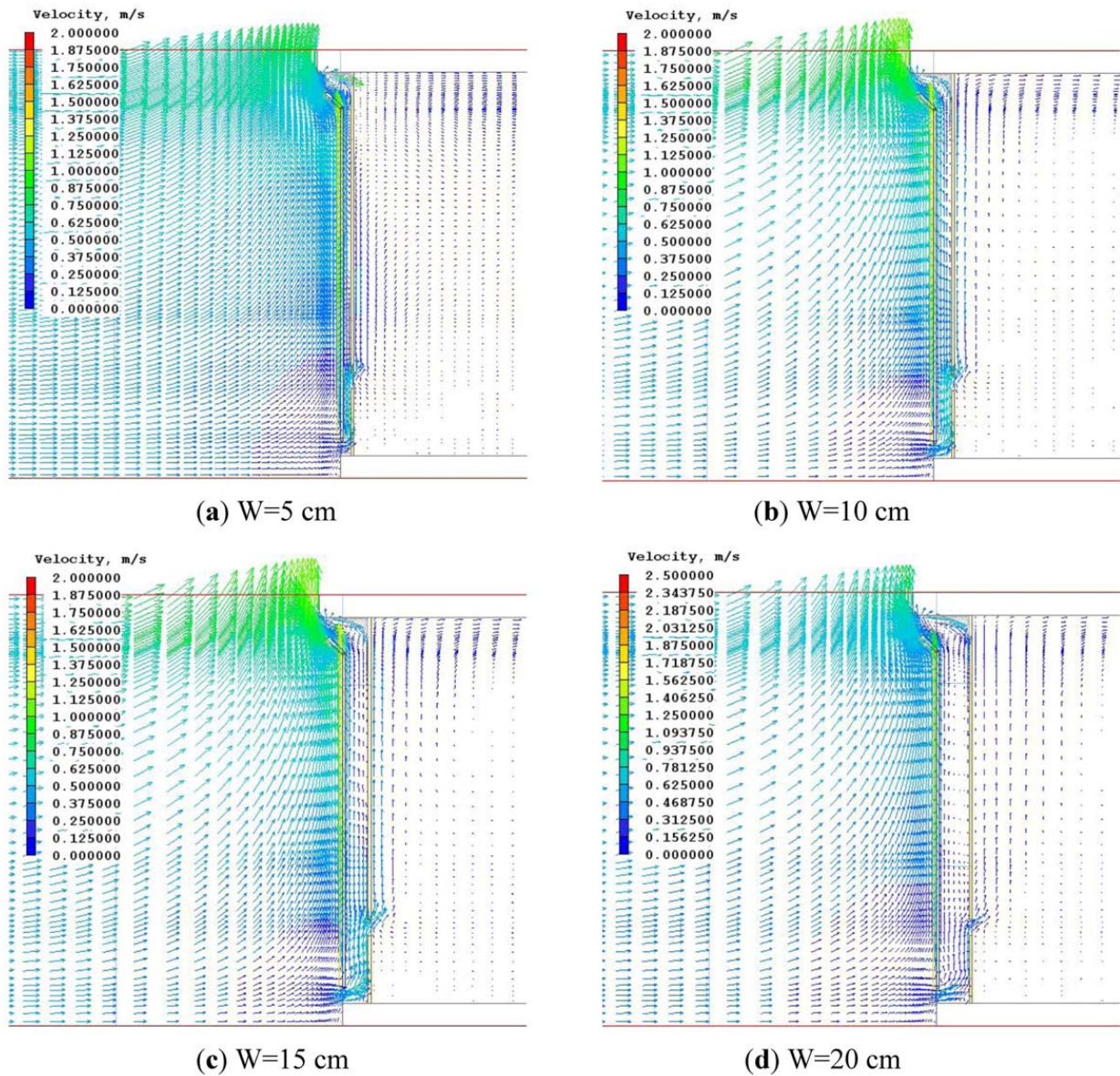
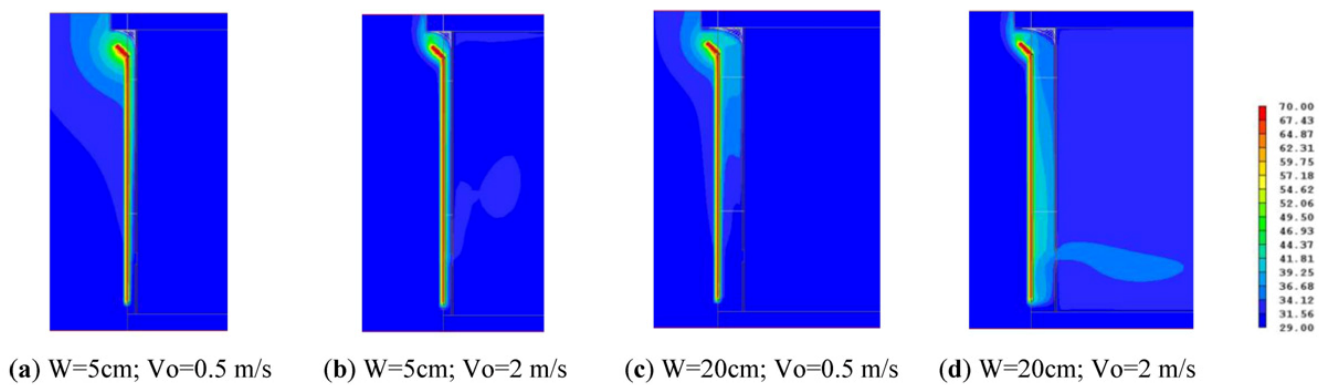
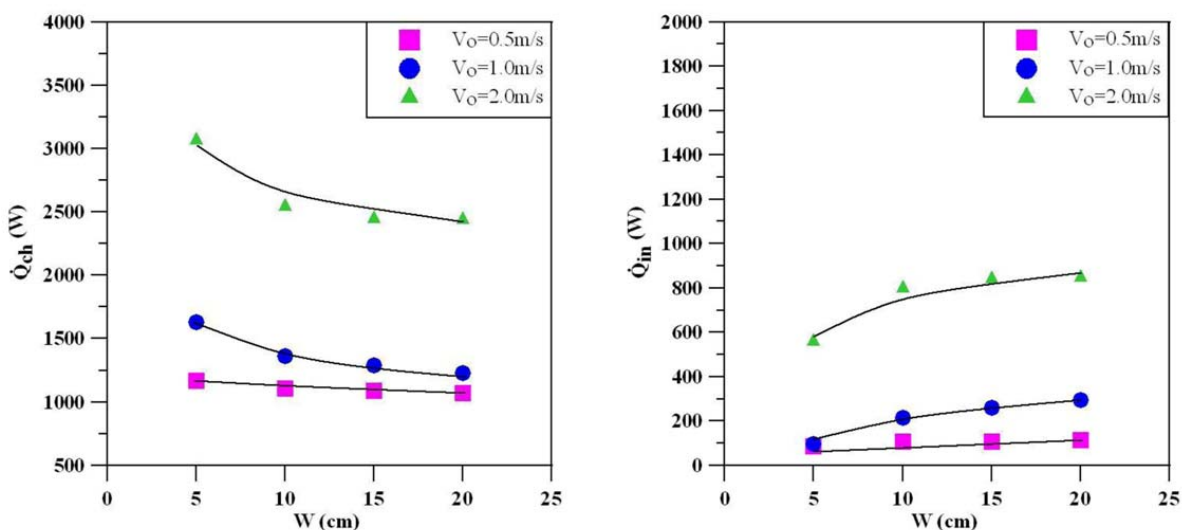


Figure 6. CFD simulations of temperature distributions (cases with $H = 45$ cm).



The effects of outdoor wind velocity and channel width on the heat removal rate and indoor heat gain, calculated using Equations (1)–(4), are shown in Figure 7. A wider airflow channel results in a lower heat removal rate for the ventilated BIPV wall. When the outdoor wind velocity was 0.5 m/s, the channel width had a minimal effect on the heat removal rate, and its average value was about 1073–1155 W. When the outdoor wind velocity was 1.0 m/s and the channel width was 5 cm, the heat removal rate was found to be at its maximum. A larger channel width results in a lower heat removal rate. An average heat removal rate value of approximately 1228–1628 W was documented. When the outdoor wind velocity was 2.0 m/s, with an airflow channel width greater than 10 cm, the heat removal rate reached an average of 2439–3065 W.

Figure 7. The effects of outdoor wind velocity (V_o) and channel width (W) on the heat removal rate (left) and indoor heat gain (right).



When the outdoor wind velocity was 0.5 m/s, the indoor heat gain of the ventilated BIPV walls was approximately 143–148 W, indicating that the indoor heat gain was not significantly affected by channel width. When the outdoor wind velocity was 1.0 m/s, the indoor heat gain was approximately 98–295 W, indicating that an increase in channel width results in an increase in indoor heat gain. When the outdoor wind velocity was 2.0 m/s, the indoor heat gain value was 558–847 W, indicating that an increase in the airflow channel width increases the indoor heat gain. When the width was greater than 10 cm, the indoor heat gain remained constant. Correlations for predicting the heat removal rate and indoor heat gain by outdoor wind velocity and channel width are $\dot{Q}_{ch} = 2203V_oW^{-1/5}$ and $\dot{Q}_{in} = 106.5V_o^{1.4}\text{Ln}(W)$, respectively. These equations are valid when the outdoor wind velocity is $V_o = 0.5\text{--}2.0$ m/s, the airflow channel width is $W = 5\text{--}20$ cm, and the indoor vent height is $H = 15\text{--}90$ cm. Details of the correlation development can be found in our previous work [11].

3.2. Reduction Ratio of the Indoor Heat Gain (η)

RC construction exterior walls commonly used in Taiwan (U value of $3.49 \text{ W/m}^2 \text{ }^\circ\text{C}$) and light steel construction (U value of $2 \text{ W/m}^2 \text{ }^\circ\text{C}$) were compared with the proposed ventilated BIPV walls. The reduction ratio of indoor heat gain (η) was calculated using Equations (5) and (6). When the outdoor

wind velocity was 0.5 m/s (with different airflow channel widths), η as compared with the RC structure was 65–73.6%. In the same instance, the reduction ratio with the steel structure was 38.8–53.9%, indicating that η was not significantly affected by the channel widths. When the outdoor wind velocity was 1.0 m/s, η of the ventilated BIPV walls was 10.5–70.2% compared with the RC structure. When the airflow width exceeded 10 cm, the additional indoor vent designed to improve indoor air quality generated an increased heat gain caused via increased indoor ventilation. This resulted in a larger indoor heat gain than observed for a steel structure. In addition, when a wider airflow channel width was used, η was –13.3~–56.3%. When the wind velocity was 2.0 m/s, the increased wind velocity increased the indoor heat gain. Thus, compared with the RC structure and steel structure, the ventilated BIPV wall generated more indoor heat gain, with η of –69.5~–157.3% and –195.7~–349%, respectively. When the airflow channel width exceeded 10 cm, η remained unchanged.

There are some cases in which it is difficult to balance energy conservation (via the ventilated BIPV walls) and ventilation benefit (via the indoor vents). Future work may explore how to strike a balanced relationship between energy conservation and indoor air quality (IAQ). Indoor illumination and acoustical environment are factors that should be taken into consideration before proposing an optimal design.

3.3. CO₂ Reduction

In this study, a ventilated BIPV wall was set up on the exterior wall facing south. Based on Taiwan's solar irradiation statistics and heat removal rates of the ventilated BIPV walls, the heat removal performance was converted to electrical energy savings (kW-h), and the reduction of CO₂ emissions was estimated. With an outdoor wind velocity of 0.5 m/s, the 2.85 m² ventilated BIPV wall was able to save 3.8–4.1 (kW-h) of electricity daily and reduce 70–76 kg of CO₂ emissions each month. When the wind velocity was 1.0 m/s, the ventilated BIPV wall was able to save 4.3–5.7 (kW-h) of electricity daily and reduce 80–107 kg of CO₂ emissions per month. Finally, when the wind velocity was 2.0 m/s, the ventilated BIPV wall was able to save 8.5–10.7 (kW-h) of electricity daily and reduce 160–201 kg of CO₂ emissions each month.

A comparison was made between a ventilated BIPV wall and a RC exterior wall. From the reduced indoor heat gain, we were able to project the reduced CO₂ emissions. This reduced heat gain was simultaneously converted to electrical energy savings (kW-h). When the outdoor wind velocity exceeded 2.0 m/s, the indoor heat gain with the ventilated BIPV wall was greater than that with the RC wall. When the outdoor wind velocity was less than 0.5 m/s, the ventilated BIPV wall was able to save 0.75–0.85 (kW-h) of electricity daily and 14–16 kg of CO₂ emissions each month. When the wind velocity was 1.0 m/s, the ventilated BIPV wall was able to save 0.3–0.8 (kW-h) of electricity daily and 5–15 kg of CO₂ emissions per month.

3.4. Induced Air Exchange of the Ventilating BIPV Wall

When the outdoor wind velocity was 0.5 m/s, the air exchange rate was not significantly affected by the channel width, with an average air exchange rate of 2.2–2.7 Air exChange rate per Hour (ACH). When the wind velocity was 1.0 m/s and 2.0 m/s, an increased channel width increased the air exchange rate, with an average of 3.5–5.4 ACH and 9.8–10.9 ACH, respectively. When the wind

velocity was between 0.5 m/s and 1.0 m/s, the air exchange rate was not significantly affected by different indoor vent heights, with an average air exchange rate of 2.2–2.7 ACH and 4.7–5.1 ACH, respectively. When the wind velocity was 2.0 m/s, a decreased indoor vent height caused the air exchange rate to increase, with an average of 9.6–12.1 ACH.

4. Conclusions

CFD simulations of flow patterns and temperature distributions of the ventilated BIPV walls were conducted under the conditions of three outdoor wind velocities, four airflow channel widths and six indoor vent heights. They show that a wider airflow channel results in a lower heat removal rate for the ventilated BIPV wall. The heat removal rate and indoor heat gain are not significantly affected by indoor vent height. The effects of outdoor wind velocity and channel width on the heat removal rate and indoor heat gain are introduced.

With an outdoor wind velocity of 0.5 m/s, 1.0 m/s, and 2.0 m/s, the 2.85 m² ventilated BIPV wall was able to save 3.8–4.1 (kW-h), 4.3–5.7, and 8.5–10.7 of electricity daily and reduce 70–76 kg, 80–107 kg, and 160–201 kg of CO₂ emissions each month, respectively.

The reduction ratio of the indoor heat gain, CO₂ reduction and induced air exchange were introduced. In some cases, the energy conservation (via ventilated BIPV walls) and ventilation benefit (via indoor vents) were unable to be balanced. Future work should explore how to obtain a balanced relationship between energy conservation and indoor air quality (IAQ).

Acknowledgements

Support from the National Science Council of ROC through grant No. NSC 98-3114-E-006-010 and NSC 100-3113-E-006-004 in this study are gratefully acknowledged.

References

1. Dubey, S.; Tiwari, G.N. Analysis of PV/T flat plate water collectors connected in series. *Sol. Energy* **2009**, *83*, 1485–1498.
2. Lai, C.M.; Huang, J.Y.; Chiou, J.S. Optimal spacing for double-skin roofs. *Build. Environ.* **2008**, *43*, 1749–1754.
3. Chang, P.C.; Chiang, C.M.; Lai, C.M. Development and preliminary evaluation of double roof prototypes incorporating RBS (Radiant Barrier System). *Energy Build.* **2008**, *40*, 140–147.
4. Afonso, C.; Oliveira, A. Solar chimneys: simulation and experiment. *Energy Build.* **2000**, *32*, 71–79.
5. Ong, K.S. A mathematical model of a solar chimney. *Renew. Energy* **2003**, *28*, 1047–1060.
6. Khedari, J.; Boonsri, B.; Hirunlabh, J. Ventilation impact of a solar chimney on indoor temperature fluctuation and air change in a school building. *Energy Build.* **2000**, *32*, 89–93.
7. Chen, Z.D.; Bandopadhyay, P.; Halldorsson, J.; Byrjalsen, C.; Heiselberg, P.; Li, Y. An experimental investigation of a solar chimney model with uniform wall heat flux. *Build. Environ.* **2003**, *38*, 893–906.

8. Del Coz Diaz, J.J.; Garcia Nieto, P.J.; Martinez Luengas, A.L.; Gonzalez Martinez, M.P. Analysis and thermal optimization of an ecological ventilated self-weighted wood panel for roofs by FVM. *Meccanica* **2010**, *45*, 619–634.
9. Abounaga, M.M. A roof solar chimney assisted by cooling cavity for natural ventilation in buildings in hot arid climates: energy conservation approach in AL-AIN city. **1998**, *14*, 357–363.
10. Spalding, D.B. *The Phoenix Encyclopedia; Concentration, Heat and Momentum (CHAM) Limited*: London, UK, 1994.
11. Lin, Y.P.; Chiang, C.M.; Lai, C.M. Energy efficiency and ventilation performance of ventilated BIPV walls. *Eng. Appl. Comput. Fluid Mech.* **2011**, in press.

© 2011 by the authors; licensee MDPI, Basel, Switzerland. This article is an open access article distributed under the terms and conditions of the Creative Commons Attribution license (<http://creativecommons.org/licenses/by/3.0/>).